ACS APPLIED MATERIALS & INTERFACES

Research Article

www.acsami.org

Relationship between Wetting Hysteresis and Contact Time of a Bouncing Droplet on Hydrophobic Surfaces

Yizhou Shen,[†] Jie Tao,*[,†] Haijun Tao, Shanlong Chen, Lei Pan, and Tao Wang

College of Material Science and Technology, Nanjing University of Aeronautics and Astronautics, Nanjing 210016, People's Republic of China

ABSTRACT: The contact time of impacting water droplets on superhydrophobic surfaces directly reflects the extent of thermal and energy conversions between the water droplet and the surface, which is also considered to be crucial to the practical applications. The purpose of this study was to reveal the relationship between the contact time and the wetting hysteresis. We designed and fabricated six classes of surfaces with different extent of hydrophobicity through modifying the microscale/nanoscale hierarchical textured titanium surfaces with 1*H*,1*H*,2*H*,2*H*-perfluorodecyltrimethoxysilane, and we filmed the contact process of the water droplet impacting on these surfaces using a high-speed camera. It can be concluded that wetting hysteresis played a significant role in determining how long the impacting water droplet can bounce off the surface, based on the interfacial wetting mechanism and the work done against the resistance force generated by contact angle hysteresis during the dynamic process.

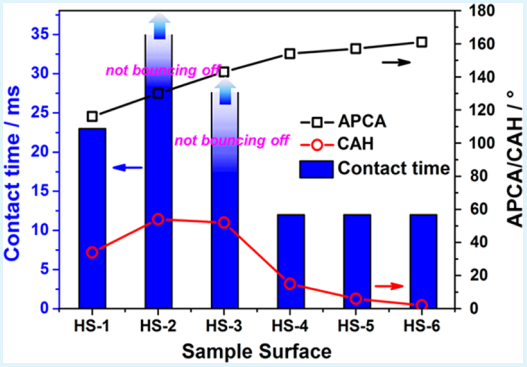

KEYWORDS: *wetting hysteresis, contact time, bouncing droplet, hydrophobic surface, superhydrophobicity*

1. INTRODUCTION

Surface nonwetting is one of the most important properties of a solid surface; it is commonly observed in our daily life, such as water droplets rolling on a lotus leaf, water striders walking on the river, and the antifogging eyes of a mosquito, etc.[1−4] These phenomena give us abundant inspirations to design functional surfaces with special nonwettability through a combination of surface chemical compositions (free energy) and surface textures. Following this principle, many researchers have devoted themselves to create and apply these surfaces.[5−7] Because of the abilities to stay dry, self-clean, reduce drag, resist icing, and prevent corrosion,[8−12] scientists believe they will greatly improve the sustainable development of resources, especially in energy and environmental aspects.

However, these nonwetting surfaces in practical situations are mostly under dynamic conditions, i.e., the water droplets continuously impacting on the surfaces.[13] The impacting water droplet (at small Weber numbers ($We \leq 10$) first spreads out to maximum deformation, and then retracts to a certain extent and bounces off the surface.[14−16] The overall contact time between the impacting water droplet and the surface is considered to be crucial, because it directly determines the extent of thermal and energy conversions in the practical application circumstances.[17] Thus, the current and future research should not only focus on designing the surface with a high apparent contact angle (APCA) and low contact angle hysteresis (CAH), but also consider reducing the contact time between the impacting water droplet and the surface.[13]

Previously, researchers have tried to perform some investigations on the contact behavior of the impacting water droplet on the various surfaces, and also gained much understanding. Liu and co-workers demonstrated that, under the same center-to-center post-spacing, surfaces with a larger apex angle could give rise to more robust pancake bouncing. Also, they developed general harmonic spring models to build the link between the contact time and surface morphology and predict the critical *We* for pancake bouncing.[18,19] Aussillous and Quéré noted that the contact angle hysteresis was a key factor to prevent the motion of the droplet on the surface, often resulting in the deposition of the liquid behind the drop.[20] Therefore, they utilized the liquid marbles (encapsulating an aqueous liquid droplet with a hydrophobic powder) to reduce the adhesion to a solid surface, consequently generating motion, under some external conditions. Furthermore, to reduce the contact time of an impacting droplet, many workers have devoted themselves to constructing extreme hydrophobic surfaces to improve surface states, also achieving some advances and showing the potential values in various industrial applications.[21,22] However, their competence in practical application cannot be thoroughly evaluated only based on the static characterizations of the apparent contact angle and the contact angle hysteresis, because we still do not grasp the underlying mechanism and relationship between the contact

Received: July 24, 2015
Accepted: September 2, 2015
Published: September 2, 2015

DOI: 10.1021/acsami.5b06754
ACS Appl. Mater. Interfaces 2015, 7, 20972−20978

time of droplet impacting on the surface and the surface nonwettability, to date. Thus, considering the practical scenarios where the nonwetting surfaces is under continuous disturbance of the environment, the contact time of the water droplet impacting on the hydrophobic or superhydrophobic surfaces should be measured and analyzed in tandem with APCA and CAH, to reveal the internal and underlying relationship.

Herein, we fully evaluate the APCA, CAH, and the contact time of a bouncing water droplet based on the designed different classes of hydrophobic surfaces. With the objective of revealing the underlying mechanism and relationship between the contact time of water droplets impacting on these surfaces and the wetting hysteresis, this study should be able to provide powerful support for the practical applications of the nonwetting surfaces.

2. EXPERIMENTAL SECTION

2.1. Materials. Ti6Al4 V titanium alloy (composition: ≤0.3 wt % Fe, ≤0.1 wt % C, ≤0.05 wt % N, ≤0.015 wt % H, ≤0.2 wt % O, 5.5−6.8 wt % Al, 3.5−4.5 wt % V, and the rest is Ti) was provided by Baoji Titanium Industry Co., Ltd., China, and cut into square substrates with sizes of 10 mm × 10 mm × 1 mm. In addition, 1*H*,1*H*,2*H*,2*H*-perfluorodecyltrimethoxysilane (FAS-17) was purchased from Tokyo Chemical Industry Co., Ltd., Japan. Other chemical reagents such as sodium hydroxide, hydrochloric acid, ethanol, and acetone are analytical grade, and provided by Sinopharm Chemical Reagent Co., Ltd., China.

2.2. Experimental Procedure. The experimental procedure invovles three processes: (i) a sand blasting treatment, (ii) a hydrothermal treatment, and (iii) fluorination modification.

2.2.1. Sand Blasting Treatment. After the Ti6Al4 V substrates were cleaned in the acetone, they were sand-blasted to construct the micrometer-scale pit structures using 150 grit alumina at 0.5 MPa for 10 s.

2.2.2. Hydrothermal Treatment. After sand blasting, the samples were placed in an autoclave containing 30 mL 1 M NaOH aqueous solution at 220 °C for a certain time. Subsequently, the samples were sufficiently rinsed with distilled water, and immersed in the 0.1 M HCl aqueous solution for 0.5 h. Furthermore, an annealing treatment at 500 °C (the heating rate of 2 °C min^{-1}) for 3 h was performed to produce TiO_2 nanowire array structures on the surface of microscale pits.

2.2.3. Fluorination Modification. Lastly, these samples were immersed in 1 wt % FAS-17 ethanol solution for 24 h and dried at 120 °C for 2 h to obtain hydrophobic sample surfaces. To make a comparative study, we therefore designed and prepared six classes of structured sample surfaces, being labeled as follows: HS-1 (smooth hydrophobic substrate); HS-2 (microscale pit surface formed by sand blasting); and HS-3, HS-4, HS-5, and HS-6 (microscale/nanoscale hierarchical structured surfaces constructed by a combination of sand blasting and hydrothermal treatment for 0.5, 1.5, 4, and 8 h, respectively).

2.3. Characterizations. A field-emission scanning electron microscopy (FE-SEM) system (Model S4800, Hitachi, Japan) was used to observe the surface morphologies of the samples. The chemical component of the surfaces was analyzed using an X-ray photoelectron spectrometer (AXIS UltraDLD, Kratos, Japan). The nonwettability of these sample surfaces was evaluated via measuring the APCA and CAH values of a 4 μL water droplet on the surfaces. APCA could be directly collected using the contact angle analyzer. CAH was calculated via the difference between the advancing contact angle (ACA) and the receding contact angle (RCA). The ACA value could be recorded by the computer, when the contact area of the water droplet on the surface changed due to the expansion of droplet. Conversely, ACA could be also achieved by shrinking the droplet.

The impact and retracting processes of the water droplet on these hydrophobic surfaces was filmed using a high-speed camera, as shown in Figure 1. The water droplet was dripped from a fixed height of 50 mm over the sample surface, and the contact time could be accurately

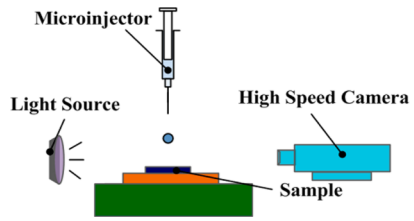

Figure 1. Schematic diagram of the impacting measurement of the water droplet on the sample surfaces.

calculated using the high-speed camera. Meanwhile, the impact velocity (V_0) of the water droplet followed the formula $v = (2gh)^{1/2}$.

3. RESULTS AND DISCUSSION

3.1. Fabrication and Composition of the Hydrophobic Surfaces. As mentioned above, fabrication of the nonwetting surfaces is based on the cooperation between surface chemical components and textures. And the surface textures are considered to be the key element for the hydrophobicity, especially the superhydrophobicity (apparent contact angle >150°; contact angle hysteresis <10°). Figure 2 illustrates the morphologies of the constructed microscale/nanoscale hierarchical textures. The sand-blasted microscale pits with an adjacent distance of ∼30 μm are evenly distributed on the substrate (see Figure 2b). Figures 2c−f show the morphologies of the one-dimensional (1D) TiO_2 nanowires planting on the

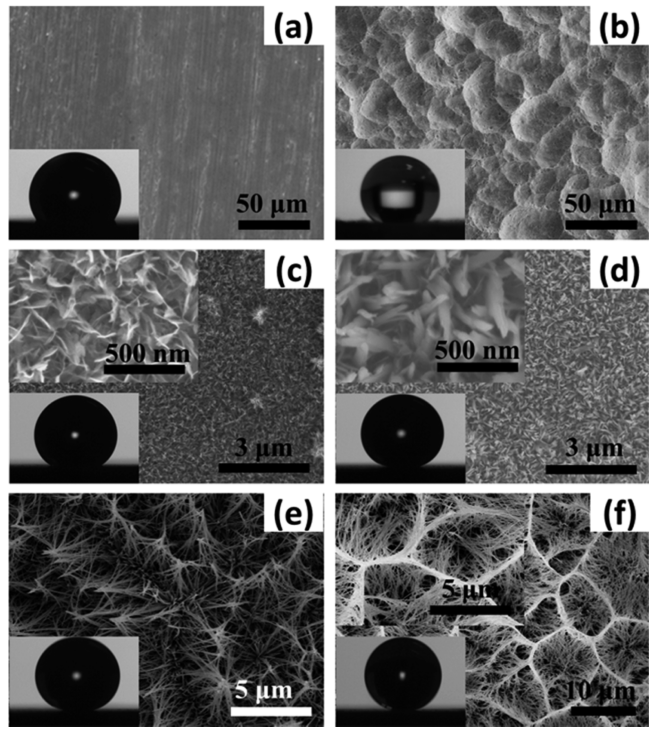

Figure 2. SEM images of these constructed microscale/nanoscale textures: (a) HS-1, smooth substrate; (b) HS-2, microscale pits formed by sand blasting; and (c) HS-3, (d) HS-4, (e) HS-5, and (f) HS-6, which represent microscale/nanoscale hierarchical structures built by a combination method of sand blasting and hydrothermal treatment for 0.5, 1.5, 4, and 8 h, respectively. The insets are the optical images of water droplets on the correspondingly prepared sample surfaces.

DOI: 10.1021/acsami.5b06754
ACS Appl. Mater. Interfaces 2015, 7, 20972−20978

surfaces of the sand-blasted microscale pits. It can be found that the generated nanowires are relatively short and small (~50 nm in diameter) for a short hydrothermal reaction time of 0.5 and 1.5 h, resulting in minor improvement in the surface structure. When the reaction time is up to 4 h, the nanowire structures experience a great change, with the length of the nanowires increasing to 2−3 μm and the endings gradually being gathered. Also, the variation of nanowire structures is further enlarged at a reaction time of 8 h.[23] According to our previous study, the features of the composite of microscale pits and nanowires synthesized with the reaction time of 8 h benefit the hydrophobicity, because of a large amount of air being trapped under the water droplets.[24]

Because of the extremely low surface free energy (~6.7 mJ m^{-2}) of FAS-17, it is considered to be an ideal choice to modify the microstructures for making the surface hydrophobic.[25−27] Figure 3 shows the XPS spectra of the sample surfaces before

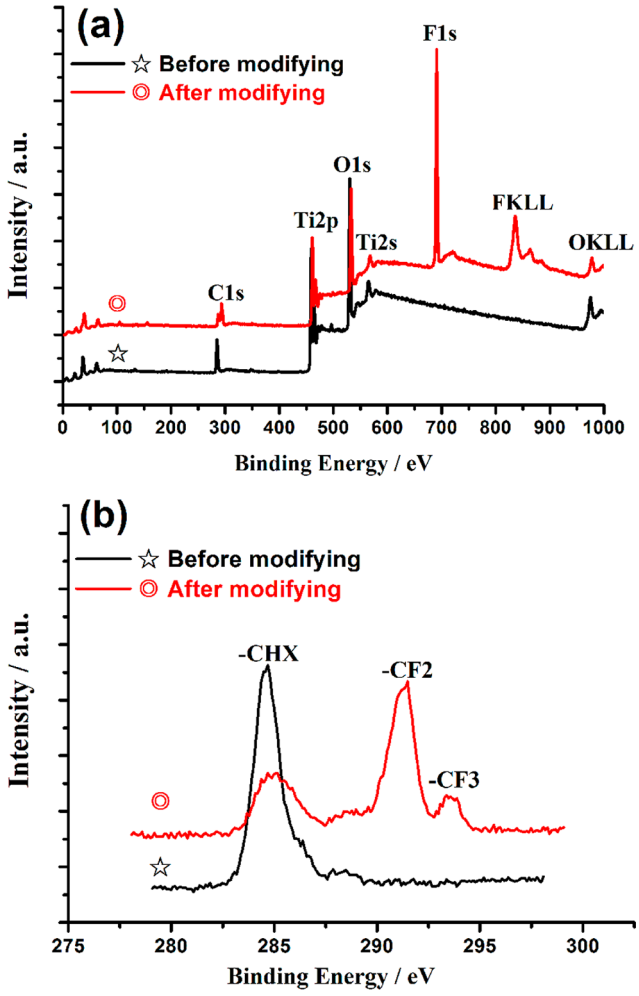

Figure 3. (a) Survey and (b) high-resolution XPS spectra of the sample surfaces.

and after fluorinating with FAS-17. It can be clearly observed that the high-intensity peaks of F 1s and FKLL are located at ~690 and 835 eV after the fluorination modification. In the high-resolution spectrum of C 1s (Figure 3b), the peaks, which respectively correspond to $-CF_2$ and $-CF_3$, are observed at the sites of ~291 eV and ~294 eV.[28] These results indicate that the FAS-17 hydrophobic groups have been successfully self-assembled to the microscale/nanoscale textured surfaces, i.e., obtaining the final hydrophobic sample surfaces. The water droplets on these sample surfaces show different shapes from hemisphere to sphere, as depicted in the insets of Figure 2.

3.2. Nonwettability. It is necessary to ascertain the nonwettability of these surfaces for revealing the relationship between the contact time of water droplets impacting on these surfaces and the wetting hysteresis. Figure 4 depicts the

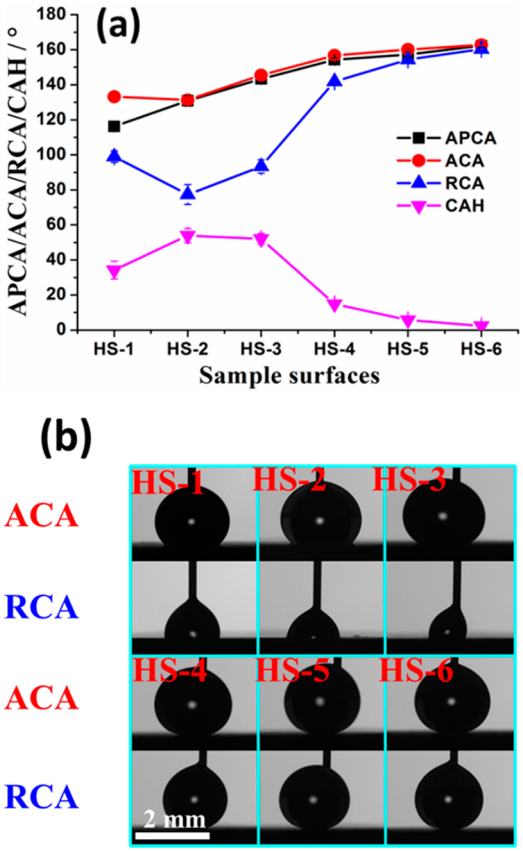

Figure 4. (a) APCA, ACA, RCA, and CAH values of a 4 μL water droplet on these sample surfaces. (b) Dynamic contact images of the water droplet expanding and shrinking on these surfaces.

measured results of APCA, CAH, ACA, and RCA. It can be found that the APCA (130°) of a water droplet on the HS-2 sample surface is higher than that on the HS-1 sample surface (116°) and the CAH also has the same trend between the two sample surfaces. The results indicate that microscale pit structure favors enhancing the APCA, but also brings disadvantageous effects on reducing the CAH. According to the Wenzel wetting state, the APCA (θ^*) of a water droplet on the microscale pit surface follows the Wenzel equation:

$$\cos\theta^* = r\cos\theta \quad (1)$$

where r is the roughness factor of the wetting area (i.e., the ratio of actual solid/liquid interfacial contact area and the apparent solid/liquid contact interfacial contact area ($r \geq 1$)), i.e., roughness factor. θ is the Young's contact angle for the smooth solid surface after the fluorination modification. The microscale pit structures on the HS-2 sample surface can effectively increase the roughness factor (r), resulting in higher APCA than that on the HS-1 sample surface. Meanwhile, the impregnating contact interface of the Wenzel wetting state

DOI: 10.1021/acsami.5b06754
ACS Appl. Mater. Interfaces 2015, 7, 20972−20978

between the water droplet and solid surface also directly determines the high CAH.

In addition, nanowire structures are hydrothermally grown on the microscale pit surface (HS-3−HS-6), causing a great change in hydrophobicity with the APCA increasing from 130° to 161° and the CAH reducing from 54° to 2°. Actually, this result is expected, since the great length:diameter ratio of the nanowire extremely increases the roughness factor, even an infinite value, leading to a very large APCA. Strictly, Wenzel wetting model should be not available in this case, because the solid/liquid contact interface has transformed to the composite contact interfaces of solid/liquid and liquid/air.[29,30] Under the action of microscale/nanoscale hierarchical structures, a large amount of air pockets are trapped under the water droplet and gradually form the Cassie wetting state, leading to the water droplet being suspended on the sample surfaces.[31−33] The APCA (θ^*) of a water droplet on the microscale/nanoscale hierarchical structured surfaces is given by[34]

$$\cos\theta^* = f_1 r \cos\theta_1 + f_1 - 1 \quad (2)$$

In this equation, θ_1 is defined as the Young's contact angles of the water droplet on the solid, f_1 is the fraction of the projected area of the solid surface that is wetted by the liquid, and r is the roughness factor of the wetting area. According to this equation, the APCA (θ^*) is mainly dependent on the contact area fraction (f_1). When the hydrothermal treatment time is up to 8 h (HS-6), the generated nanowires and microscale pit structures collaboratively induce a large amount of air pockets, resulting in very small f_1 (~10%),[35,36] and a high APCA of 161°, as well as a low CAH of 2°. For a relatively short hydrothermal treatment time (0.5−1.5 h), the nanowires are short and small, therefore causing a surface transition wetting state (i.e., metastable Cassie wetting) between the Wenzel and Cassie wetting states.[34,37] The APCA values of the water droplets on the HS-3 and HS-4 sample surfaces are 140°−150°, and the CAHs are still very high.

3.3. Contact Time of the Droplet Impacting on the Surfaces. To measure the contact time of water droplets impacting on these surfaces, we filmed the contact process using a high-speed camera. Figure 5 depicts the impact processes of the water droplets (initial diameter D_0 = 2 mm, impact velocity V_0 = 1 m s^{-1}) on these sample surfaces. It can be clearly seen that the processes of the water droplet spreading out to an almost-uniform coating on the six sample surfaces are almost the same, because of the same initial kinematic parameters of the water droplet. However, there is an obvious difference in the retracting processes among these sample surfaces. It takes ~23 ms for the impacting water droplet on the HS-1 sample surface to complete the overall process, and leave a tiny droplet. In comparison to the HS-1 sample surface, the HS-2 sample surface displays a higher hydrophobic performance with APCA = 130° and CAH = 54°. However, the impacting water droplet cannot bounce off the surface, because of the strong adhesion. For the HS-3 sample surface, although the hydrophobicity is further enhanced with the APCA reaching 143° and the CAH reducing to 52°, the impacting water droplet still cannot bounce off the surface. When the water droplets impact on the HS-4, HS-5, and HS-6 sample surfaces, it takes ~13 ms to complete the overall impact process, and the water droplets can successfully bounce off the three sample surfaces.

At this point, we urgently want to know what causes the variation of the contact processes (contact time) of the water droplet impacting on these sample surfaces, APCA, or CAH? For this purpose, we rearrange the relative data for better analysis, as shown in Figure 6. It can be visually observed that

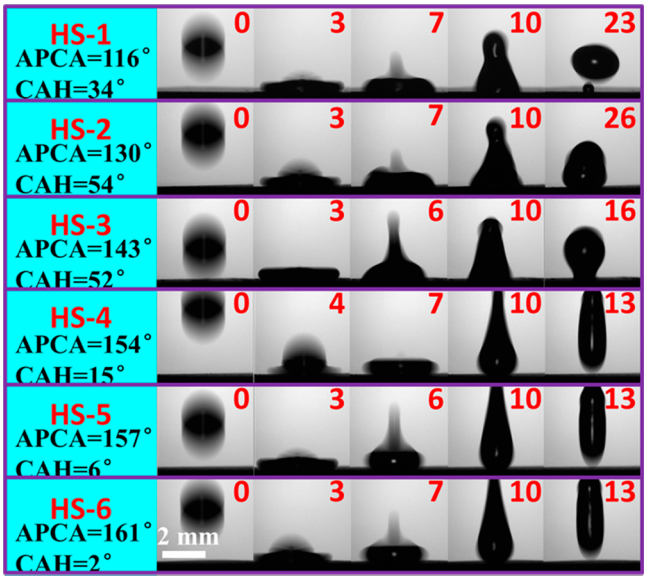

Figure 5. Impact processes of the water droplets (initial diameter D_0 = 2 mm, impact velocity V_0 = 1 m s^{-1}) on these sample surfaces. Values shown in red are presented in units of milliseconds (ms).

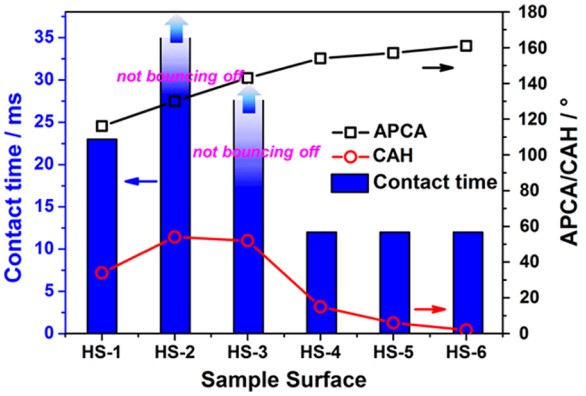

Figure 6. Relationship between the contact time of water droplets impacting on these surfaces and the hydrophobicity. Therein, the impacting water droplet on the HS-2 and HS-3 sample surfaces cannot bounce off the surfaces, as shown by the arrows.

the impacting water droplets only on the HS-2 and HS-3 sample surfaces cannot bounce off the surfaces, as the APCA of the water droplet on these surfaces gradually increases. Also, we find that the CAH of the water droplets on the HS-2 and HS-3 sample surfaces are greater than those on other sample surfaces (i.e., HS-1, HS-4, HS-5, and HS-6). According to the changing trends of contact time and CAH, perhaps the CAH of the droplet on the solid surface has significant influence on the contact time of the water droplet impacting on the surface.

3.4. Relationship between Wetting Hysteresis and Contact Time. Setting a liquid droplet in motion requires non-negligible forces to overcome the resistance force generated by CAH, and often results in the deposition of liquid behind the drop.[19] As analyzed above, the overall contact process of a water droplet impacting on a solid surface consists of the spreading and retracting processes. In order to qualitatively

DOI: 10.1021/acsami.5b06754
ACS Appl. Mater. Interfaces 2015, 7, 20972−20978

analyze the relationship between the wetting hysteresis and the work done against the resistance force generated by CAH, we assume that, in the spreading process to the maximal diameter (D_{max}), the water droplet moves forward with the advancing contact angle (θ_A). When the water droplet retracts, the receding contact angle (θ_R) is available (see Figure 7). Thus,

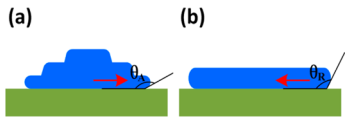

Figure 7. Dynamic process of the water droplet impacting on the solid surface: (a) spreading process with the advancing contact angle (ACA), and (b) retracting process with the receding contact angle (RCA).

the work done (W_1, W_2) in spreading and retracting processes against the resistance force generated by CAH is given by

$$W_1 = \int_0^{1/2D_{max}} f_A \pi r \, dr = \frac{1}{8}\pi {D_{max}}^2 \sigma_{lg} |\cos\theta - \cos\theta_A| \quad (3)$$

$$W_2 = \int_0^{1/2D_{max}} f_R \pi r \, dr = \frac{1}{8}\pi {D_{max}}^2 \sigma_{lg} |\cos\theta - \cos\theta_R| \quad (4)$$

where f_A and f_R are the resistance forces to spreading and retracting by the CAH, respectively, and σ_{lg} is the liquid/gas interfacial tension. The overall work done against the resistance force generated by CAH in the dynamic process can be obtained as

$$W = W_1 + W_2 = \frac{1}{8}\pi {D_{max}}^2 \sigma_{lg} (\cos\theta_R - \cos\theta_A) \quad (5)$$

Furthermore, the relationship between the maximal diameter (D_{max}) and the initial diameter (D_0) can be followed by[38]

$$\frac{D_{max}}{D_0} = \sqrt{\frac{We + 12}{3(1 - \cos\theta^*) + 4\frac{We}{\sqrt{Re}}}} \quad (6)$$

where the Weber number (We) and the Reynolds number (Re) are constant in this work. Thus, combining eqs 3, 4, 5, and 6, we can draw the following conclusion:

$$W \propto \frac{\cos\theta_R - \cos\theta_A}{1 - \cos\theta^*} \quad (7)$$

During the water droplet impacting the solid surface, the higher APCA value and the lower CAH value will result in a less work done against the resistance force generated by CAH. Thus, the water droplets impacting on the HS-4, HS-5, and HS-6 sample surfaces require very little kinetic energy to overcome the work done, showing the impacting water droplet rapidly rebounding off the surfaces (the tiny differences of the contact time among the three sample surfaces are not apparent due to the limited frames of the camera). Comparison of the rebounding properties of the water droplets on HS-2 and HS-3 sample surfaces shows that the water droplet can rebound off the smooth HS-1 sample surface with a longer contact time, because of the lower CAH value.

To further reveal the relationship between the contact time of the water droplet impacting on the hydrophobic surfaces and the wetting hysteresis, we also analyze the contact mechanism between the impacting water droplets and the typical structured hydrophobic surfaces (see Figure 8). As mentioned previously,

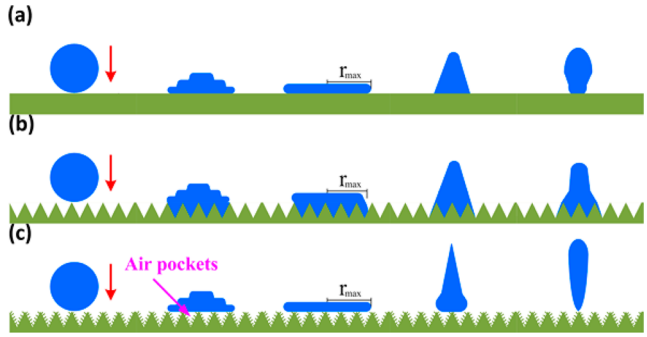

Figure 8. Schematic diagrams of contact interfaces between the impacting water droplets and the typical structured hydrophobic surfaces: (a) smooth substrate; (b) microscale pits formed by sand blasting; and (c) microscale/nanoscale hierarchical structures constructed by a combination of sand blasting and hydrothermal treatment.

the water droplet on the microscale pit surface follows the Wenzel wetting state, resulting in the impregnating contact interface. When the water droplet impacts on the microscale pit surface at a certain velocity, it can rapidly fill the microscale structures without any air. Thus, the outside atmospheric pressure can effectively prevent the impacting water droplet from bouncing off the surface, causing the stable Wenzel wetting state.[39,40]

Conversely, the impacting water droplet on the microscale/nanoscale hierarchical structured hydrophobic surface can easily bounce off the surface. Under the action of the microscale/nanoscale hierarchical structures, a large amount of air can be trapped under the water droplet and form the nonimpregnating contact interface, following the Cassie wetting state.[41] Although the water droplet impacts on the microscale/nanoscale hierarchical structured hydrophobic surface at a certain velocity, the air trapped under the water droplet still cannot be pushed out, because of the locking-gas ability from the extremely large roughness factor of the surface.[42,43] The Cassie–Baxter state possibly changes to a metastable state in the spreading process. However, when the water droplet starts to retract, the metastable state gradually transfers to the stable Cassie–Baxter state again. In this case, the impacting water droplet can easily bounce off the surface without resistance, and the water droplet on the surface has a low CAH value. Thus, in comparison with APCA, CAH can better reflect the contact time of the water droplet impacting on the surface.

4. CONCLUSION

In summary, we designed and fabricated six classes of hydrophobic surfaces by modifying the microscale/nanoscale hierarchical textures on Ti6Al4 V substrate with FAS-17. Comparing with the smooth hydrophobic substrate surface, although the microscale pit structured surface displayed a high apparent contact angle (APCA), the contact angle hysteresis (CAH) also increased, because of the impregnating contact interface, leading to the outside atmospheric pressure effectively preventing the impacting water droplet from bouncing off the surface. However, the impacting water droplet on the microscale/nanoscale hierarchical structured surface could be easily bounced off the surface, because of the extremely low CAH caused by the trapped air under the water droplet. Also, we comparatively analyzed the work done against the resistance force generated by CAH, indicating that the water droplets

DOI: 10.1021/acsami.5b06754
ACS Appl. Mater. Interfaces 2015, 7, 20972–20978

impacting on surfaces with the high APCA and the low CAH require very little kinetic energy to overcome the work done, and rapidly rebound off the surfaces.

AUTHOR INFORMATION

Corresponding Author

*Tel./Fax: +86-25-52112911. E-mail: taojie@nuaa.edu.cn.

Author Contributions

†Y. Shen and J. Tao contributed equally to this work.

Notes

The authors declare no competing financial interest.

ACKNOWLEDGMENTS

The authors gratefully acknowledge the financial support of the National Science Foundation of China (Nos. 51475231, 51205196, and 51202112), a Project Funded by the Priority Academic Program Development of Jiangsu Higher Education Institutions, the Jiangsu Innovation Program for Graduate Education (No. KYLX_0261), Open Fund of Jiangsu Key Laboratory of Materials and Technology for Energy Conversion (No. MTEC-2015M04), and the Fundamental Research Funds for the Central Universities (No. NJ20150027).

REFERENCES

(1) Style, R. W.; Dufresne, E. R. Static Wetting on Deformable Substrates, from Liquids to Soft Solids. *Soft Matter* **2012**, *8*, 7177−7184.

(2) Liu, M.; Zheng, Y.; Zhai, J.; Jiang, L. Bioinspired Super-antiwetting Interfaces with Special Liquid−Solid Adhesion. *Acc. Chem. Res.* **2010**, *43*, 368−377.

(3) Watson, G. S.; Gellender, M.; Watson, J. A. Self-Propulsion of Dew Drops on Lotus Leaves: A Potential Mechanism for Self Cleaning. *Biofouling* **2014**, *30*, 427−434.

(4) Liu, K.; Yao, X.; Jiang, L. Recent Developments in Bio-inspired Special Wettability. *Chem. Soc. Rev.* **2010**, *39*, 3240−3255.

(5) Yan, Y. Y.; Gao, N.; Barthlott, W. Mimicking Natural Superhydrophobic Surfaces and Grasping the Wetting Process: A Review on Recent Progress in Preparing Superhydrophobic Surfaces. *Adv. Colloid Interface Sci.* **2011**, *169*, 80−105.

(6) Lai, Y. K.; Huang, J. Y.; Gong, J. J.; Huang, Y. X.; Wang, C. L.; Chen, Z.; Lin, C. J. Superhydrophilic−Superhydrophobic Template: A Simple Approach to Micro- and Nanostructure Patterning of TiO_2 Films. *J. Electrochem. Soc.* **2009**, *156*, 480−484.

(7) Wen, L.; Tian, Y.; Jiang, L. Bioinspired Super-wettability from Fundamental Research to Practical Applications. *Angew. Chem., Int. Ed.* **2015**, *54*, 3387−3399.

(8) Lai, Y.; Tang, Y.; Gong, J.; Gong, D.; Chi, L.; Lin, C.; Chen, Z. Transparent Superhydrophobic/superhydrophilic TiO_2-Based Coatings for Self-cleaning and Anti-fogging. *J. Mater. Chem.* **2012**, *22*, 7420−7426.

(9) Chen, Y.; Chen, S.; Yu, F.; Sun, W.; Zhu, H.; Yin, Y. Fabrication and Anti-corrosion Property of Superhydrophobic Hybrid Film on Copper Surface and its Formation Mechanism. *Surf. Interface Anal.* **2009**, *41*, 872−877.

(10) Daniello, R. J.; Waterhouse, N. E.; Rothstein, J. P. Drag Reduction in Turbulent Flows over Superhydrophobic Surfaces. *Phys. Fluids* **2009**, *21*, 085103.

(11) Boinovich, L. B.; Emelyanenko, A. M. Anti-icing Potential of Superhydrophobic Coatings. *Mendeleev Commun.* **2013**, *23*, 3−10.

(12) Ruan, M.; Li, W.; Wang, B.; Deng, B.; Ma, F.; Yu, Z. Preparation and Anti-icing Behavior of Superhydrophobic Surfaces on Aluminum Alloy Substrates. *Langmuir* **2013**, *29*, 8482−8491.

(13) Ramachandran, R.; Sobolev, K.; Nosonovsky, M. Dynamics of Droplet Impact on Hydrophobic/Icephobic Concrete with the Potential for Superhydrophobicity. *Langmuir* **2015**, *31*, 1437−1444.

(14) Bird, J. C.; Dhiman, R.; Kwon, H. M.; Varanasi, K. K. Reducing the Contact Time of a Bouncing Drop. *Nature* **2013**, *503*, 385−388.

(15) Miljkovic, N.; Enright, R.; Nam, Y.; Lopez, K.; Dou, N.; Sack, J.; Wang, E. N. Jumping-Droplet-Enhanced Condensation on Scalable Superhydrophobic Nanostructured Surfaces. *Nano Lett.* **2013**, *13*, 179−187.

(16) Tsai, P.; Pacheco, S.; Pirat, C.; Lefferts, L.; Lohse, D. Drop Impact upon Micro- and Nanostructured Superhydrophobic Surfaces. *Langmuir* **2009**, *25*, 12293−12298.

(17) Tran, T.; Staat, H. J. J.; Susarrey-Arce, A.; Foertsch, T. C.; van Houselt, A.; Gardeniers, H. J. G. E.; Prosperetti, A.; Lohse, D.; Sun, C. Droplet Impact on Superheated Micro-structured Surfaces. *Soft Matter* **2013**, *9*, 3272−3282.

(18) Liu, Y.; Whyman, G.; Bormashenko, E.; Hao, C.; Wang, Z. Controlling Drop Bouncing Using Surfaces with Gradient Features. *Appl. Phys. Lett.* **2015**, *107*, 051604.

(19) Liu, Y.; Moevius, L.; Xu, X.; Qian, T.; Yeomans, J. M.; Wang, Z. Pancake Bouncing on Superhydrophobic Surfaces. *Nat. Phys.* **2014**, *10*, 515−519.

(20) Aussillous, P.; Quéré, D. Liquid Marbles. *Nature* **2001**, *411*, 924−927.

(21) Shen, Y.; Tao, J.; Tao, H.; Chen, S.; Pan, L.; Wang, T. Superhydrophobic Ti6Al4V Surfaces With Regular Array Patterns for Anti-icing Applications. *RSC Adv.* **2015**, *5*, 32813−32818.

(22) Hu, C.; Liu, S.; Li, B.; Yang, H.; Fan, C.; Cui, W. Micro-/Nanometer Rough Structure of a Superhydrophobic Biodegradable Coating by Electrospraying for Initial Anti-Bioadhesion. *Adv. Healthcare Mater.* **2013**, *2*, 1314−1321.

(23) Tang, Y.; Zhang, Y.; Deng, J.; Wei, J.; Tam, H. L.; Chandran, B. K.; Dong, Z.; Chen, Z.; Chen, X. Mechanical Force-Driven Growth of Elongated Bending TiO_2-based Nanotubular Materials for Ultrafast Rechargeable Lithium Ion Batteries. *Adv. Mater.* **2014**, *26*, 6111−6118.

(24) Shen, Y.; Tao, J.; Tao, H.; Chen, S.; Pan, L.; Wang, T. Nanostructures in Superhydrophobic Ti6Al4V Hierarchical Surfaces Control Wetting State Transitions. *Soft Matter* **2015**, *11*, 3806−3811.

(25) He, M.; Zhang, Q.; Zeng, X.; Cui, D.; Chen, J.; Li, H.; Wang, J.; Song, Y. Hierarchical Porous Surface for Efficiently Controlling Microdroplets' Self-Removal. *Adv. Mater.* **2013**, *25*, 2291−2295.

(26) He, J.; Li, H.; Liu, X.; Qu, X. Fabricating Superamphiphobic Surface with Fluorosilane Glued Carbon Nanospheres Films. *J. Nanosci. Nanotechnol.* **2013**, *13*, 1974−1979.

(27) Wu, Y.; Liu, K.; Su, B.; Jiang, L. Superhydrophobicity-Mediated Electrochemical Reaction Along the Solid−Liquid−Gas Triphase Interface: Edge-Growth of Gold Architectures. *Adv. Mater.* **2014**, *26*, 1124−1128.

(28) Lai, Y. K.; Lin, C. J.; Wang, H.; Huang, J. Y.; Zhuang, H. F.; Sun, L. Superhydrophilic−Superhydrophobic Micropattern on TiO_2 Nanotube Films by Photocatalytic Lithography. *Electrochem. Commun.* **2008**, *10*, 387−391.

(29) Ju, J.; Zheng, Y.; Jiang, L. Bioinspired One-Dimensional Materials for Directional Liquid Transport. *Acc. Chem. Res.* **2014**, *47*, 2342−2352.

(30) Liu, K. S.; Yao, X.; Jiang, L. Recent Developments in Bio-inspired Special Wettability. *Chem. Soc. Rev.* **2010**, *39*, 3240−3255.

(31) Whyman, G.; Bormashenko, E. How to Make The Cassie Wetting State Stable? *Langmuir* **2011**, *27*, 8171−8176.

(32) Spori, D. M.; Drobek, T.; Zürcher, S.; Spencer, N. D. Cassie-State Wetting Investigated by Means of a Hole-to-Pillar Density Gradient. *Langmuir* **2010**, *26*, 9465−9473.

(33) Bormashenko, E.; Pogreb, R.; Stein, T.; Whyman, G.; Erlich, M.; Musin, A.; Machavariani, V.; Aurbach, D. Characterization of Rough Surfaces with Vibrated Drops. *Phys. Chem. Chem. Phys.* **2008**, *10*, 4056−4061.

(34) Marmur, A. Wetting on Hydrophobic Rough Surface: To Be Heterogeneous or Not To Be? *Langmuir* **2003**, *19*, 8343−8348.

(35) Miwa, M.; Nakajima, A.; Fujishima, A.; Hashimoto, K.; Watanabe, T. Effects of the Surface Roughness on Sliding Angles of Water Droplets on Superhydrophobic Surfaces. *Langmuir* **2000**, *16*, 5754−5760.

DOI: 10.1021/acsami.5b06754
ACS Appl. Mater. Interfaces 2015, 7, 20972−20978

(36) Wang, J.; Liu, M.; Ma, R.; Wang, Q.; Jiang, L. *In Situ* Wetting State Transition on Micro- and Nanostructured Surfaces at High Temperature. *ACS Appl. Mater. Interfaces* **2014**, *6*, 15198−15208.
(37) Bico, J.; Thiele, U.; Quéré, D. Wetting of Textured Surfaces. *Colloids Surf., A* **2002**, *206*, 41−46.
(38) Pasandideh-Fard, M.; Qiao, Y. M.; Chandra, S.; Mostaghimi, J. Capillary Effects During Droplet Impact on A Solid Surface. *Phys. Fluids* **1996**, *8*, 650−659.
(39) Zheng, Q. S.; Yu, Y.; Zhao, Z. H. Effects of Hydraulic Pressure on the Stability and Transition of Wetting Modes of Superhydrophobic Surfaces. *Langmuir* **2005**, *21*, 12207−12212.
(40) Jung, Y. C.; Bhushan, B. Dynamic Effects of Bouncing Water Droplets on Superhydrophobic Surfaces. *Langmuir* **2008**, *24*, 6262−6269.
(41) Bormashenko, E. Why Does The Cassie-Baxter Equation Apply? *Colloids Surf., A* **2008**, *324*, 47−50.
(42) Kim, Y. D.; Shin, J. H.; Cho, J. Y.; Choi, H. J.; Lee, H. Nanosized Patterned Protective Glass Exhibiting High Transmittance and Self-Cleaning Effects for Photovoltaic Systems. *Phys. Status Solidi A* **2014**, *211*, 1822−1827.
(43) Barletta, M.; Vesco, S.; Tagliaferri, V. Self-cleaning and Self-Sanitizing Coatings on Plastic Fabrics: Design, Manufacture and Performance. *Colloids Surf., B* **2014**, *120*, 71−80.

DOI: 10.1021/acsami.5b06754
ACS Appl. Mater. Interfaces 2015, 7, 20972−20978